January 1990

Underestimation of Visual Texture Slant by Human Observers: A Model

M. R. Turner
University of Pennsylvania

Ruzena Bajcsy
University of Pennsylvania

G. L. Gerstein
University of Pennsylvania

University of Pennsylvania Department of Computer and Information Science Technical Report No. MS-CIS-90-02.

Underestimation of Visual Texture Slant by Human Observers: A Model

Abstract

The perspective image of an obliquely inclined textured surface exhibits shape and density distortions of texture elements which allow a human observer to estimate the inclination angle of the surface. However, since the work of Gibson (1950) it has been known that, in the absence of other cues, humans tend to underestimate the slant angle of the surface, particularly when the texture is perceived as being "irregular."

The perspective distortions which affect texture elements also shift the projected spatial frequencies of the texture in systematic ways. Using a suitable local spectral filter to measure these frequency gradients, the inclination angle of the surface may be estimated. A computational model has been developed which performs this task using distributions of outputs from filters found to be a good description of simple cell receptive fields. However, for "irregular" textures the filter output distributions are more like those of regular textures at shallower angles of slant, leading the computational algorithm to underestimate the slant angle. This behavioral similarity between human and algorithm suggests the possibility that a similar visual computation is performed in cortex.

Comments

University of Pennsylvania Department of Computer and Information Science Technical Report No. MS-CIS-90-02.

Underestimation Of Visual Texture Slant By Human Observers: A Model

MS-CIS-90-02
GRASP LAB 200

M.R. Turner
R. Bajcsy
G.L. Gerstein

Department of Computer and Information Science
School of Engineering and Applied Science
University of Pennsylvania
Philadelphia, PA 19104-6389

January 1990

Underestimation of Visual Texture Slant by Human Observers: A model

M. Turner[%#], G. Gerstein[%] and R. Bajcsy[#]

[%]Department of Physiology
[#]Department of Computer and Information Science
University of Pennsylvania
Philadelphia, Pennsylvania 19104

ABSTRACT

The perspective image of an obliquely inclined textured surface exhibits shape and density distortions of texture elements which allow a human observer to estimate the inclination angle of the surface. However, since the work of Gibson (1950) it has been known that, in the absence of other cues, humans tend to underestimate the slant angle of the surface, particularly when the texture is perceived as being "irregular."

The perspective distortions which affect texture elements also shift the projected spatial frequencies of the texture in systematic ways. Using a suitable local spectral filter to measure these frequency gradients, the inclination angle of the surface may be estimated. A computational model has been developed which performs this task using distributions of outputs from filters found to be a good description of simple cell receptive fields. However, for "irregular" textures the filter output distributions are more like those of regular textures at shallower angles of slant, leading the computational algorithm to underestimate the slant angle. This behavioral similarity between human and algorithm suggests the possibility that a similar visual computation is performed in cortex.

INTRODUCTION

A textured surface viewed at an oblique inclination will exhibit certain systematic distortions in texture element shape and density. These distortions may be used to recover shape information about the surface such as its curvature or the angle between the surface and the observer's line of sight. However, it has been known since the experiments of Gibson in 1950 that, in the absence of other cues, a human subject will tend to make systematic errors in this type of problem. When shown a perspective projection of a textured planar surface, observers tend to perceive it as having a steeper or more perpendicular inclination than it actually has. Moreover, it has also been found that the amount of underestimation tends to be greater for textures which are perceived as being "irregular". Although this perceptual tendency has been replicated in a variety of experimental studies (Gruber and Clark, 1956; Clark et al., 1956; Flock and Moscatelli, 1964; Braunstein, 1968), few models have been offered in explanation (Perrone, 1980). In this paper we describe a computational model which uses as its low level operator a filter found to be a good and economical description of simple cell receptive fields. Two dimensional distributions of filter outputs are used to estimate the inclination of a textured surface. However, for "irregular" textures the distributions of filter output are much like the those of regular textures at shallower angles of slant, leading the computational algorithm to underestimate the slant angle. This underestimation error is likely to affect the performance of any system (animal or machine) attempting

to determine the inclination of a textured surface from local spectral measurements.

There are two types of systematic distortion which occur in a perspective transformation of an inclined textured plane. First, as the plane recedes into the distance, texture elements on the surface will project to progressively smaller areas in the image plane and, of course, their projected density will also increase. This is a distance effect: areas further away on the textured plane project to smaller areas in the image. Second, as the texture recedes into the distance the angle between the observer's line of sight and the plane becomes more acute. This causes an additional distortion which compresses the image of a texture element along the direction of slant of the textured plane. Unlike the distance effect which compresses both length and width, this distortion only compresses the dimension along which the texture slants away from the viewer. This is known as the foreshortening effect.

The distortions which affect the dimensions of projected texture elements will also affect the local spectra of their projection. The amount of scaling, however, differs with respect to both location in the image plane and orientation (because of the foreshortening effect). Hence, the projection of the spectral components in a texture will vary in frequency by different amounts in different locations and along different image orientations. By measuring the local spectrum at many locations these variations may be used to estimate the amount and direction of the slant of the original uniformly textured plane.

Local spectral analysis for the detection of texture gradients was developed within a machine vision context by Bajcsy and Lieberman (1976). In this work windowed Fourier transforms were used to detect changes in spatial frequency peaks across the image of slanted natural textures such as ocean waves or fields of grass. To detect these systematic spatial variations in projected spatial frequencies, the low level operators applied directly to the image must afford some degree of spatial and spectral resolution. Although Bajcsy and Lieberman used windowed Fourier transforms, there are a number of other filtering operations which could serve the same purpose. For the texture gradient work described in this paper, the 2D Gabor function has been used. This filter form has been shown to be a good model for the 2 dimensional receptive field structure of real neurons in the visual system.

The form and purpose of the receptive fields of cells in visual cortex has been extensively studied and discussed for thirty years, with particular attention given to the primary visual cortex or V1. The structure of the receptive fields of simple cells and their contribution to the computational functions of vision became a topic of intense debate throughout the 1970's. Two general models were proposed. In the first, simple cells were viewed as performing a kind of spatially local bar or edge detection (Hubel and Wiesel, 1959, 1962; Marr, 1982). The second model suggested a more global spatial frequency analysis of visual information similar to a Fourier transform (Enroth-Cugell and Robson, 1966; Campbell and Robson, 1968). In the early 1980's a compromise in the form of a filter type first suggested by Dennis Gabor (1946) in a signal processing context was proposed (Daugman, 1980, 1985; Marcelja, 1980; MacKay, 1981). There is an uncertainty principle which limits the resolution simultaneously attainable in space and spatial frequency by a linear filter. It was suggested that Gabor filters which, under certain norms, achieve the maximum possible joint resolution allowed by the theory, matched the receptive field profiles of simple cells. Daugman (1985) extended the theory to show that the joint optimization criterion also holds for the two dimensional form of Gabor filters. Physiological experiments have demonstrated that the 2D Gabor filter is, indeed, a good model for simple cell receptive fields (Jones and Palmer, 1987a, 1987b; Jones et al. 1987).

GABOR FILTERS

A 2D Gabor filter may be visualized as the product of a sinusoidal plane wave of some frequency and orientation with a 2 dimensional elliptical Gaussian. The filters used in this work are discrete realizations of the following function:

$$G_{\phi}(x,y) = \exp\left[-\frac{(x - x_c)^2 + (y - y_c)^2}{2\sigma^2} \right] \sin \omega\left[x \cos\alpha - y \sin\alpha + \phi \right] \qquad (1)$$

where

x_c and y_c are the center locations of the Gabor filter Gaussian envelope.

σ is the standard deviation of the Gaussian envelope.

ω is the frequency of the sinusoidal plane wave.

α is the orientation of the plane wave.

ϕ is its phase.

The characteristics and selectivities of a filter are determined by these variables with ω and α the frequency-orientation peaks, and σ the spatial size of the Gaussian (and thereby also the frequency bandwidth). For simplicity, only circularly symmetric Gaussians have been used in this work. ϕ determines the phase of the filter. For each set of frequency, orientation and size parameter choices, a pair of filters is generated differing in spatial phase by 90 degrees (see figure 1).

Each filter is applied to an image in a number of overlapping regions. Each such region may be thought of as something like a receptive field. A correlation is made of each filter with the image material falling within such a region. From the resulting values obtained using the two filters differing only in phase, an amplitude or output value is computed as:

$$A = \sqrt{V_{\phi_1}^2 + V_{\phi_2}^2} \qquad (2)$$

where V_{ϕ_1} and V_{ϕ_2} are the values computed from the same image region using the filters of different phase. (Further details are available in Turner, 1986.)

The Fourier transform of a 2D Gabor filter is a pair of elliptical Gaussians displaced positively and negatively from the origin by the amount of the filter modulation frequency and rotated from the horizontal axis by the orientation angle of the filter. The standard deviations of the frequency Gaussians are inversely related to those of the spatial Gaussian. (Because the spatial Gaussian envelopes of the Gabor filters used in this paper are circularly symmetric, so are the corresponding frequency envelopes.)

PERSPECTIVE IMAGING AND FILTER OUTPUTS

The imaging model for this work, shown in figure 2, is a much simplified but adequate approximation of that occurring in the eye. A textured surface with slant θ (Stevens, 1983) is imaged by a pinhole camera with focal length f.

Figure 3a shows a perspective projection of a sine wave grating slanted 50 degrees. The perspective distortions of the spectral component of a slanted textured surface will induce smooth local frequency variations from region to region in the image plane. Consequently, the output of a particular Gabor filter pair will also vary smoothly as the correlation between the filters' modulation frequency and that of the projected spectral component differs. Figure 3b shows the amplitude distribution of one Gabor filter pair for the sine wave grating of figure 3a. The output measured at each region (26 regions per dimension have been used in this example) has been shown as a small square at the same location as the image region from which the measurement was taken and with an intensity proportional to the measured output. In this example the amplitude peak is the bright band extending across the center of the figure with the amplitudes falling off smoothly above and below the peak.

For illustrative simplicity, we may reduce the dimensionality of the examples by considering only a central vertical slice through the filter output distribution. In figure 3c filter outputs for 6 regions along this slice are shown as small x's. With a knowledge of the perspective dimensions, the texture frequency being projected and the parameters of the Gabor filter pair, we may evaluate an equation (described in Turner et al., 1989a) at each point along the vertical slice line to predict the filter output that would be measured at each such point in the image. The result is shown in figure 3c as the continuous line which quite accurately fits the 6 values actually measured from the grating image. The curve along the different locations of the vertical image slice forms a peak because the perspective distortions project the grating frequency to different points across the Gaussian frequency response of the measuring filter pair.

This may be graphically illustrated in the two dimensional spatial frequency plot shown in figure 3d (only the positive quadrant is shown). The curved line represents the spatial frequencies to which the grating projects at each spatial point along the vertical image slice. The 6 spatial locations have been denoted by the horizontal bars across the line with the bottom most image region at the bottom (lowest frequency part) of the curve. Notice that, because of the foreshortening effect, the vertical component of the frequency increases faster than the horizontal. Therefore, the line curves upward slightly and the distance between bars increases in the higher frequencies (the upper part of the grating image).

Three contours of the filter pairs' Gaussian frequency response are shown as the concentric circles (.25, .5 and .75 of maximum amplitude). The dot in the center represents the filters' modulation frequency. Each point along the curve intersects the filters' Gaussian at some location. The filter output at the corresponding position in the image is approximated by the value of the Gaussian at that point.

Decreasing the slant angle has the effect of also decreasing the spatial frequency gradient in the image plane with a corresponding flattening of the Gabor filter output curve. Figure 3c shows the output curves for the original grating at a 50 degree slant and another grating at a shallower 36 degree slant. Similarly, as the slant angle increases the peak becomes sharper.

The shape and sharpness of the filter output curve is an indicator of angle of slant of the original textured surface. For the grating examples shown above, all of the parameters are known and the smooth curves in figures 3c and 4b may be generated by computing the predicted output from these parameters

(including the known slant of the grating) at different spatial locations in the image. However, it is the inverse problem of identifying the slant of textured surfaces in the natural world that must be solved in a biological or machine vision system. The distributions of filter outputs from the image are available and it is the surface inclination which must be determined.

Two machine techniques have been used to evaluate the slant starting from Gabor filter outputs. The first method involves comparison between the two dimensional distributions of filter outputs measured from an image and those predicted with the amplitude equation for some initial choice of angle. The angle of slant is then adjusted iteratively in small steps by a hill climb algorithm, always choosing new parameters in the direction of lower error. An algorithm to perform this computation has been written and is the subject of another paper (Turner, et al., 1989a). Slant estimates calculated with this algorithm will be used in the texture examples shown later in the paper.

The second technique is more suggestive from a physiological perspective since it is unlikely that a neural assembly could estimate slant angle by explicit evaluation of the nonlinear equation used by the algorithm. Nevertheless, complicated algorithmic transformations may be realized by sets of receptive fields which represent specific instances of the transformation. Cells with receptive fields describing the filter amplitude distributions for particular slant angles would be templates for specific instances of the equation. These cells would, by their firing rates, denote the degree to which the amplitude distributions of a number of lower level cells with Gabor like receptive fields match expected spatial distributions for particular slant angles. Using a back-propagation algorithm (Rumelhart et al. 1986), receptive fields with the necessary properties have been generated by a layered neural network simulation and are the subject of another paper (Turner, et al., 1989b).

TEXTURES CONTAINING MULTIPLE SPECTRAL COMPONENTS

Most textures encountered in the real world are quite unlike the sine wave grating examples shown in the previous section. Textures often contain variations in the contrasts and frequencies of spectral components from region to region. A more critical problem, however, is that textures may be composed of a number of different spatial frequencies, many times relatively closely spaced and of similar contrast. Because of the spectral uncertainty inevitably associated with a filter of finite spatial extent, the amplitude measured with a particular filter often represents contributions of several different frequencies, rather than just one as in the sine wave example. As the perspective distortions shift these spectral components, the fraction contributed by each to the filter output will vary. This has the effect of distorting the output curves in ways which often appear consistent with those of lower slant angles.

For example, suppose the single spectral value of the sine wave grating (figure 3a) is replaced by 4 frequencies spaced around the single grating frequency. Figure 4a shows the texture composed of the 4 separate frequencies at the same 50 degree slant angle as the grating. The plot of figure 4c shows the path of each frequency component along the vertical image slice. The output of the single Gabor filter pair is approximated by the sum of influences of each component:

$$O = \sum_{i=1}^{4} A_i \tag{3}$$

Output curves for the 1 frequency and 4 frequency examples are shown together in figure 4b. The 4 frequency curve is broader and flatter than the one for the sine wave grating and is almost identical to

the single frequency grating at a 36 degree angle of slant in figure 3c. (In fact, for this image the algorithm computed a slant of 33.1 degrees.) A visual system attempting to estimate slant angle from local spectral filter outputs would be more likely to underestimate the slant of such a texture. The 4 frequency texture gives most viewers the impression of a smaller angle of inclination.

REALISTIC TEXTURE EXAMPLES

The texture examples which follow are taken from Brodatz (Brodatz, 1966; Weber, 1986). The original texture photographs were digitized perpendicular to the camera. Using standard computer graphics techniques, slanted instances of the textures were created by mapping the perpendicular digitized images onto imaginary inclined planar surfaces and then applying a perspective transformation algorithm. This procedure avoids complications such as occlusion of texture elements, shadows, or differences in lighting and reflectance at different slant angles, and thereby makes it easier to make an unbiased comparison of filter output distributions from the same material at different angles.

Filters were applied to images of these textured surfaces slanted at angles of 0, 10, 20, 30, 40 and 50 degrees. For each slant angle specification and texture, two images were generated as input to the algorithm. The first image contains the slant and perspective transformation applied to the digitized texture in its original form. For the second, the original image was rotated 180 degrees before the slant and perspective transformation was applied. By averaging the algorithm slant estimates for both members of the image pair the effect of systematic variations in the original texture on the frequency gradients may be reduced.

In a biological system, it is probable that a variety of filters at different frequencies, orientations and positions would be available for parallel application to the image. In simulation on a sequential machine, application of many filters is both expensive and unnecessary. The frequency gradient information is most evident in the subset of filters which match the frequencies of the projected spectral components; other filters have relatively low outputs. For the examples which follow, filter specifications have been selected by identification of the peaks in the global discrete Fourier transforms (DFT) of the images. Several filters bracketing projected frequencies of these peaks are then applied to the images. Six filter pairs (figure 1) were used, with an orientation of 90 degrees and wavelengths spanning 8 to 18 pixels in 2 pixel increments.

The image of a brick wall slanted at a 30 degree angle is shown in figure 5c. The "regularity" of this texture is evident in the DFT of a windowed region from the center of the image (figure 5b). The iterative algorithm described in the previous section has been applied to this image and for this 30 degree slant produced an estimate of 28.73 degrees. Figure 8 shows in graphical form the program estimates for the 6 differently slanted brick wall images.

Figure 6c shows a raffia weave texture at the same 30 degree slant. The windowed DFT is shown in figure 6b. This texture, while it contains a spectral peak representing the periodicities of the weave, also contains a number of other components. In DFT's of several other image regions, the variation and contrast changes in the weave obscure the peak, lending a more irregular appearance. The program estimate for this example, at 24.27 degrees, is lower than for the similarly slanted brick wall. For this texture, the program usually underestimated the slant of each image by an amount somewhat greater than that for the brick wall (figure 8).

As the density of spectral components around a peak becomes greater, the filter output curve also becomes flatter, suggesting that certain textures should produce little or no perception of slant. If human perception of texture slant is based, in part, upon local spectral gradients, then in the absence of other cues, such textures should appear to have nearly perpendicular or uncertain slant, both to the algorithm and to humans. Figure 7c shows the image of a calfskin texture slanted at the same 30 degree angle. Its windowed DFT (figure 7b) shows a dense cloud of spectral components forming a relatively broad peak. Although the texture contains a distinct pattern of texture elements forming the grain of the hide, little or no impression of slant is apparent in the image. The algorithm applied to this figure estimated a slant of 1.90 degrees; similar values were estimated for other angles of slant for this material. Thus, the program heavily underestimates the slant of each calfskin image (figure 8).

DISCUSSION

The spectral properties of real textured surfaces can affect the spatial distributions of individual filter outputs in ways which decrease the accuracy of slant estimates. In particular, the multiple, closely spaced frequency values characterizing a texture of "irregular" appearance can alter the distributions of individual filter outputs consistent with more regular textures at shallower angles of slant. A system relying upon local spectral values alone for slant estimation would be likely to misperceive an irregularly textured surface as having in inclination closer to perpendicular than it actually has.

A number of variations were tried in the choice of filter frequencies, number of filter values used by the algorithm, termination criteria, etc. Although the exact slant estimates differed somewhat from run to run, they all replicated the tendency to underestimate slant of the calfskin texture more than the raffia, and the raffia more than the brick wall.

Gibson and others (Gibson, 1979; Gibson and Cornsweet, 1952; Epstein and Park, 1964; Perrone, 1980) have suggested that the perception of slant is not an absolute quality, but a relative one affected by the occluding edges of the viewing window and the relationship of the window to other parts of the room and to gravity. While this may explain the human tendency to underestimate the slant of all textured stimuli, it does not provide much insight into the different levels of accuracy associated with regular and irregular textures. Obviously, the computer algorithm has no awareness of these additional geographical factors. Consequently, it produced more accurate slant estimations for the very regular brick wall texture than did the human subjects in Gibson's experiment (1950). However, the algorithm replicated the tendency toward increasing inaccuracy with textural irregularity, suggesting that several different mechanisms may underlie the underestimation of surface slant in human observers and that these are not easily separated in psychophysical experiments.

For local spectral slant estimation a visual system requires more information to make its estimate than the distributions of filter outputs taken individually. When the computer algorithm fits sets of parameters to the outputs of one filter type (i.e. only one frequency, orientation, and bandwidth), its slant estimate is frequently opposite the correct value. In other words, a textured surface which actually slants away from the viewer at the top by a certain angle is perceived by the algorithm as sloping toward the viewer at the top by a similar angle. (In fact, one of the subjects in Gibson's experiment perceived the slant of an irregular texture stimulus in exactly this way. Gibson, 1950, p. 379) This occurs because there are two minima in the error surface for a filter taken alone, one for the positive slant angle and one for the negative one. A visual system attempting to estimate the slant parameter by minimizing error on this kind of surface may be trapped in the reversal minimum. The problem may be corrected

by requiring simultaneous parameter evaluation over several filters which differ slightly in frequency. However, this only increases the tendency to underestimate the slant of irregular textures by altering the relationships between outputs of different frequency filters. This kind of multiple receptor constraint is known to exist in other perceptual modalities (Erickson, 1963, 1974) and for the present application reduces the likelihood of reversed inclination estimates (This is discussed further in Turner, et al., 1988a).

Even with a variety of local spectral constraints, the accurate analysis of surface properties certainly requires a multitude of other mechanisms. The circumstances carefully created in the particular psychophysical experiments mentioned above are highly artificial. The visual system has been deprived of most of the natural environmental cues to surface inclination such as stereopsis, convergence of surface borders, relative movement of the texture elements with the motion of the observer, hue changes with increasing distance, etc. It is probable that the tendency to underestimate surface slant is not a critical deficiency, because the mechanism which makes inclination estimates from perspective projections almost never operates alone. In normal conditions, all of the analysis mechanisms very likely operate together for improved accuracy and reliability. Nevertheless, the psychophysical experiments do suggest that, however inaccurately, the human visual system has the means of perceiving slant solely from perspective distortions of texture. If it exists in humans, it also seems likely that this ability exists in the visual systems of other primates and mammals; the associated mechanisms may profitably be sought at the neuronal level.

Electrophysiological experiments indicate that visual cells frequently operate by application of receptive fields to image material. These cells may be organized in a hierarchical manner to extract increasingly complex and subtle information from the image. At higher visual levels the receptive fields may be sufficiently complicated that an understanding of their purpose is difficult if not impossible without a model of the computation being performed (Hopfield and Tank 1986; Sejnowski et al. 1988). This poses significant problems for the design and interpretation of physiological experiments.

A companion paper describes theoretical investigations into receptive fields for the perception of surface inclination. A 3-layer neural network simulation with a learning algorithm was employed to suggest physiologically plausible mechanisms for this ability. The receptive fields which emerged from this study are organized like the ordinary spatial orientation detectors commonly found in studies of visual cortex, but defined along an unusual set of stimulus dimensions. In the studies performed so far we have used one dimension of space and one of frequency. It is in this space-frequency coordinate system that the receptive fields of the hidden layer neural network elements display a specific orientation. In other words, these network elements are sensitive to the presence of particular different spatial frequencies at particular different locations along the spatial axis. The rate at which the frequency preference changes with spatial location (corresponding to the angle of "orientation" in this coordinate system) determines the surface slant to which the element responds. Cells with this receptive field organization have not been described in the physiological literature. However, it is also unlikely that an experiment to detect such cells would be designed without the basis of a predictive theoretical model. We are currently investigating the degree to which such a receptive field system reproduces the slant underestimation behavior.

The model described in this paper replicates the human tendency to underestimate the slant angle of textured planar surfaces. This does not by any means guarantee that a similar computational process is occurring in cortex. Entirely different methods of texture analysis may exhibit similar behavior. While the current model is suggestive, considerably more work is required to fully understand the perception of textured surface inclination in humans and animals. As previously mentioned, research is underway

to extend the models to the level of neuronal mechanisms. As these and other computational models are tested in physiological experiments, visual processes such as texture gradient perception may be better understood.

ACKNOWLEDGMENTS

Support for this research was provided by ONR N00014-87-K-0766 and AFOSR 88-0296. We thank Paul M. Gochin for introducing us to the problem of textured surface slant underestimation.

REFERENCES

Bajcsy R, Lieberman L (1986) Texture gradient as a depth cue. *Computer Graphics and Image Processing*5:52-67

Braunstein ML (1968) Motion and texture as sources of slant information. *J of Exp Psychol*78:247-253

Brodatz P (1966) *Textures, a photographic album for artists and designers.* Dover, New York

Campbell FW, Robson JG (1968) Application of Fourier analysis to the visibility of gratings. *J Physiol (London)*197:551-566

Clark WC, Smith AH, Ausma Rabe (1956) The interaction of surface texture, outline gradient and ground in the perception of slant. *Canad J Psychol*10:1-8

Daugman JG (1980) Two-dimensional spectral analysis of cortical receptive field profiles. *Vision Res*20:847-856

Daugman JG (1985) Uncertainty relation for resolution in space, spatial frequency and orientation optimized by two-dimensional visual cortical filters. *J Opt Soc Am A*2:1160-1169

Enroth-Cugell C, Robson JG (1966) The contrast sensitivity of retinal ganglion cells of the cat. *J Physiol (London)*187:517-552

Epstein W, Park J (1964) Examination of Gibson's psychophysical hypothesis. *Psychological Bulletin*62:180-196

Erickson RP (1963) Sensory neural patterns and gustation. In: Zotterman Y (ed) *Olfaction and Taste* pages 205-213 MacMillan, New York

Erickson RP (1974) Parallel "population" neural coding in feature extraction. In: Schmitt FO, Worden FG (eds) *The Neurosciences: Third Study Program* pages 155-169. MIT Press, Cambridge, Mass.

Flock H, Moscatelli A (1964) Variables of surface texture and accuracy of space perceptions. *Perceptual and Motor Skills*19:327-334

Gabor D (1946) Theory of communication. *J IEE (London)*93:429-457

Gibson JJ (1950) The perception of visual surfaces. *Am J Psychol*63:367-384

Gibson JJ (1979) *The ecological approach to visual perception.* Houghton Mifflin, Boston

Gibson JJ, Cornsweet J (1952) The perceived slant of visual surfaces - optical and geographical. *J Exp Psych*44:11-15

Gruber HE, Clark WC (1956) Perception of slanted surfaces. *Perceptual and Motor Skills*6:97-106

Hubel DH, Wiesel TN (1959) Receptive fields of single neurons in the cat's striate cortex. *J Physiol (London)*148:574-591

Hubel DH, Wiesel TN (1962) Receptive fields, binocular interaction and functional architecture in the cat's visual cortex. *J Physiol (London)*160:106-154

Hopfield JJ, Tank DW (1986) Computing with neural circuits: a model. *Science*,

Jones JP, Palmer LA (1987) An evaluation of the two-dimensional Gabor filter model of simple receptive fields in cat striate cortex. *J Neurophysiology*58:1233-1258

Jones JP, Palmer LA (1987) The two-dimensional spatial structure of simple receptive fields in cat striate cortex. *J Neurophysiology*58:1187-1211

Jones JP, Stepnowski A, Palmer LA (1987) The two-dimensional spectral structure of simple receptive fields in cat striate cortex. *J Neurophysiology*58:1212-1232

Kulikowski JJ, Marcelja S, Bishop PO (1982) Theory of spatial position and spatial frequency relations in the receptive fields of simple cells in the visual cortex. *Biol Cybern*43:187-198

MacKay DM (1981) Strife over visual cortical function. *Nature (London)*289:117-118

Marcelja S (1980) Mathematical description of the responses of simple cortical cells. *J Opt Soc Am*70:1297-1300

Marr D (1982) *Vision.* W.H. Freeman, San Francisco

Perrone JA (1980) Slant underestimation: a model based on the size of the viewing aperture. *Perception*9:285-302

Rumelhart DE, Hinton GE, Williams RJ (1986) Learning internal representations by error propagation. In: Rumelhart DE, McClelland JL (eds) *Parallel Distributed Processing: Exploring the Microstructures of Cognition.* pages 318-364. MIT Press, Cambridge, Mass.

Sejnowski TJ, Koch C, Churchland PS (1988) Computational Neuroscience. *Science*241:1299-1307

Stevens K (1983) Slant-tilt: The visual encoding of surface orientation. *Biol Cybern*46:183-195

Turner MR (1986) Texture discrimination by gabor functions. *Biol Cybern*55:71-82

Turner MR, Bajcsy R, Gerstein GL (1989) Estimation of textured surface inclination by parallel local spectral analysis. (submitted)

Turner MR, Salganicoff M, Gerstein GL, Bajcsy R (1989) Receptive fields for the determination of textured surface inclination. (submitted)

Weber AG (1986) Image data base. *Technical Report USC SIPI Report 101* , University of Southern California, Signal and image processing institute

FIGURE CAPTIONS

Figure 1: The set of 12 2D Gabor filters in the top half of the figure are the ones used in calculating inclination of all the natural texture examples which follow in the paper. The set contains 6 frequencies (8 - 18 pixel wavelengths in 2 pixel increments), all at 90 degree orientation with 2 phases (0 and 90 degrees) for each frequency specification. All filters have a bandwidth of 1.5 octaves, thereby making them scalings and rotations of the two larger filters (shown to provide a more detailed view of the smaller filters actually used) in the bottom half of the figure.

Figure 2: Perspective imaging model. A textured planar surface with coordinate system (u,v) is distance d from a pinhole camera with a flat image plane, coordinate system (x,y) and focal length f. The inclination of the textured surface is indicated by the angle θ.

Figure 3: (a) The image of a surface containing an oriented (60 degrees) sine wave grating slanted 50 degrees from the vertical will exhibit systematic local changes in spatial frequency. (All images are 512 by 512 pixels with gray scale values from 0 to 255.) Although the vertically oriented filters shown in figure 1 are not ideal for this grating, the algorithm slant estimate for this image was 46.3 degrees. (b) Application of a particular 2D Gabor filter pair to the perspective sine wave image of the previous figure. The amplitude of the filter pair (indicated by the gray level intensity with the highest amplitude indicated by white) varies from location to location in the image depending upon the local match between the projected sine wave frequency in the image plane and the frequency -- orientation of the Gabor filter. (c) The x's represent 6 amplitude values selected at different locations along a vertical slice through this distribution. (The amplitude scale is in arbitrary units. The spatial location scale is in pixels.) The continuous curve through the x's has been computed using an equation which describes the approximate amplitude of the Gabor filter pair from the inclination and frequency parameters. To illustrate the change in curve shape with different inclinations, a second distribution slice has been shown for a grating slanted 36 degrees. This curve is considerably broader and flatter than the one for the 50 degree inclination. The distribution curves have a peaked shape because the perspective distortions project the grating frequency to different points along the Gaussian frequency response of the measuring filter pair. (d) This is best illustrated in a two dimensional spatial frequency plot (only the positive quadrant has been shown). Three contours of the filter pairs' Gaussian frequency response are shown as the concentric circles (.25, .5 and .75 of maximum amplitude). The line represents the projected spatial frequencies of the 50 degree slanted grating at different spatial locations along the image slice. The 6 tic marks are the spatial locations represented by the x's of figure c. The amplitude of the Gabor filter pair at each spatial location is approximated by the Gaussian value at the corresponding point in this plot.

Figure 4: (a) Natural textures often contain a number of closely spaced frequencies which vary locally from region to region. This figure is composed of the sum of four spatial frequencies spaced around the single grating frequency of figure 3a. (b) In this case, the amplitude of a single Gabor filter pair represents the sum of influences of each separate frequency component. As shown in this figure, this produces an amplitude distribution curve which is broader and flatter, more closely resembling the single frequency curve of figure 3c at a 36 degree slant. In fact, when run against this multiple frequency image, the algorithm computed a slant of 33.1 degrees. (c) In this spatial frequency plot, the path of each frequency component along the vertical image slice is shown relative to the Gabor filter Gaussian frequency response. The amplitude of the Gabor filter pair at each spatial location is now approximated by the sum of the four Gaussian values at each point.

Figure 5: (a) Image of a brick wall perpendicular to the line of sight. (b) The discrete Fourier transform (DFT) of a small windowed section (130 x 130 pixels) of the center of (a) shows a strong spectral peak representing the periodicities of the brick pattern. (For the purposes of photographic reproduction, a nonlinear gray scale was used on the DFT figures.) (c) Using standard computer graphics techniques the image of (a) is slanted and then given a perspective projection. This shows the brick wall slanted 30 degrees. The algorithm slant estimate for this image was 28.73 degrees.

Figure 6: (a) Image of a perpendicular raffia weave texture. (b) The windowed DFT of this image shows a more complicated spectral pattern. (c) The raffia image slanted 30 degrees. The algorithm estimate was 24.27 degrees.

Figure 7: (a) A calfskin texture perpendicular to the viewer. (b) Its windowed DFT shows a cloud of spectral components without the clearly defined peaks evident in the textures of figures 5 and 6. (c) The perspective image of the calfskin slanted 30 degrees gives almost no impression of inclination. The algorithm estimate for this image was 1.9 degrees.

Figure 8: A graph showing algorithm estimates for the three natural textures slanted 0, 10, 20, 30, 40, and 50 degrees. While the algorithm produced accurate slant estimates for the brick wall texture (most estimates fall very near the diagonal line representing perfect accuracy), it tended to underestimate the slant of most inclinations of the raffia. The calfskin texture has sufficient spectral complexity that the algorithm is incapable of determining its slant with any degree of accuracy.

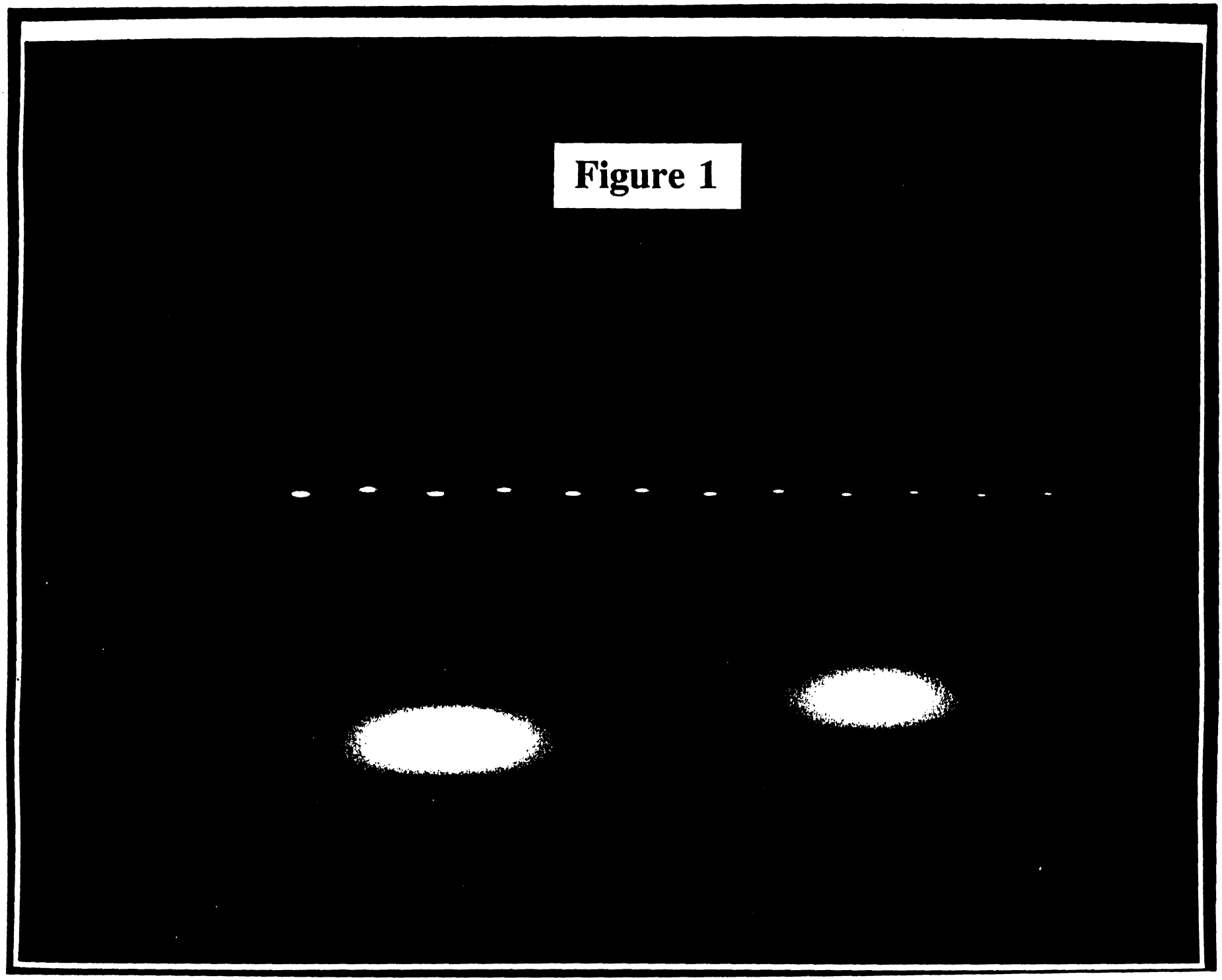
Figure 1

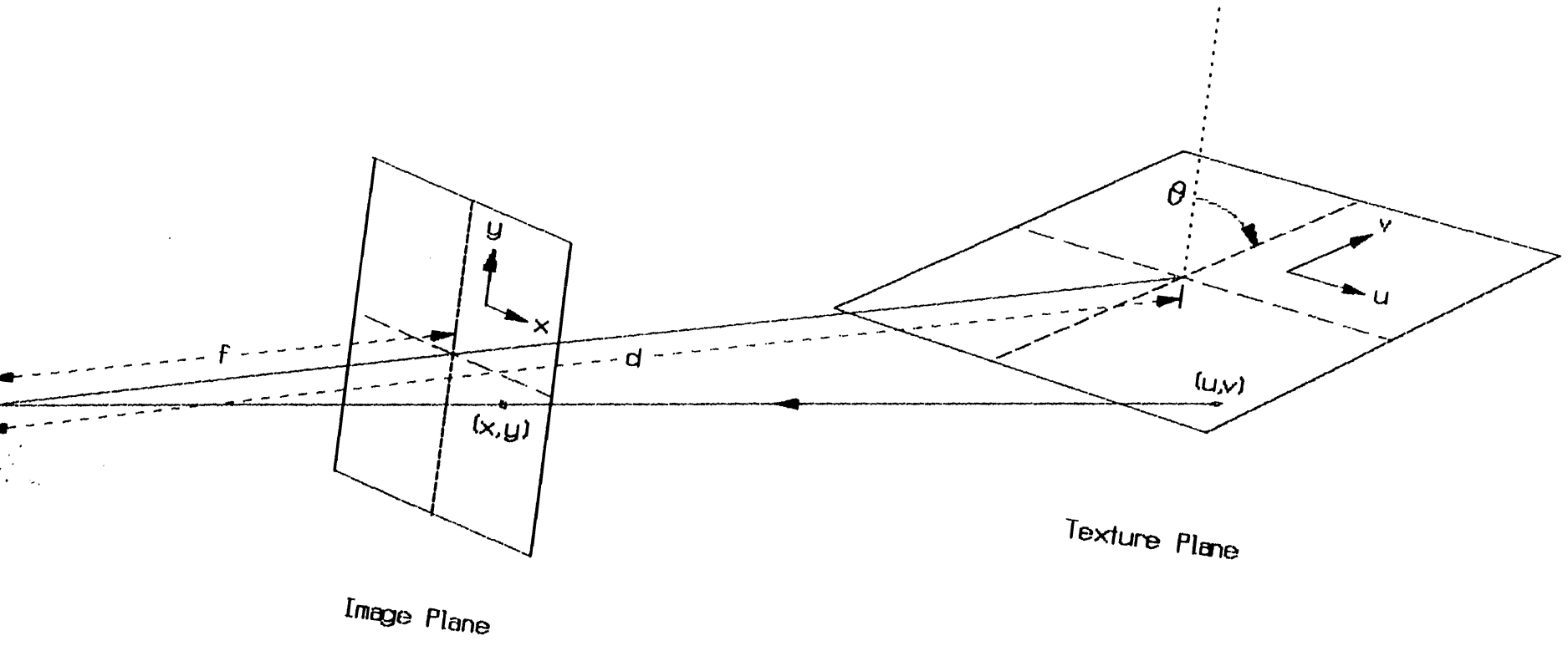

Figure 2

Figure 3a

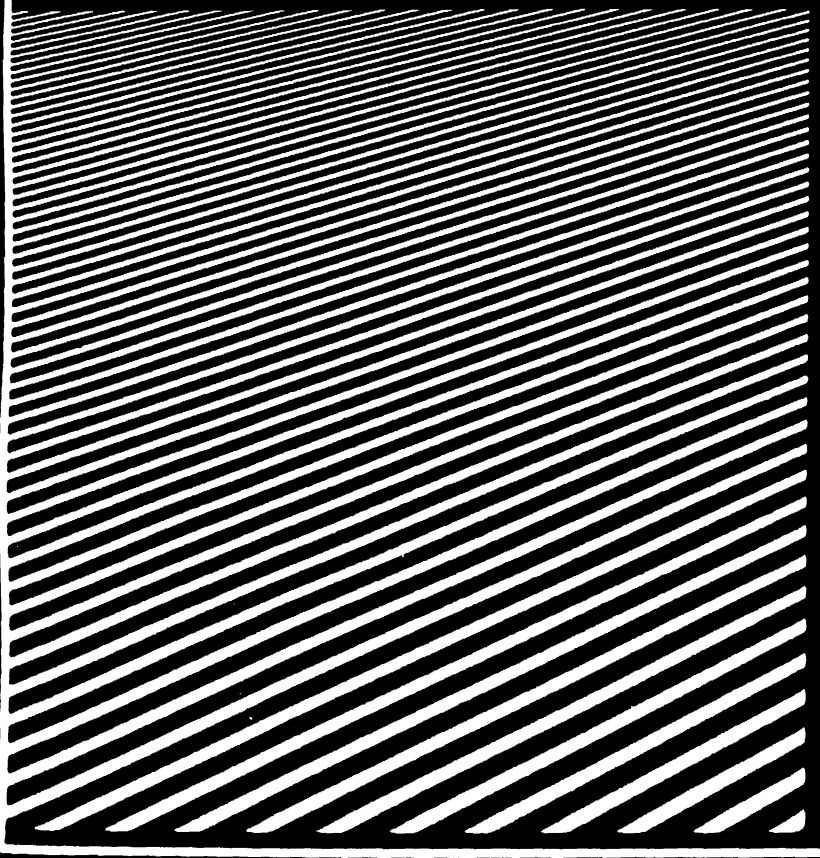

Figure 4a

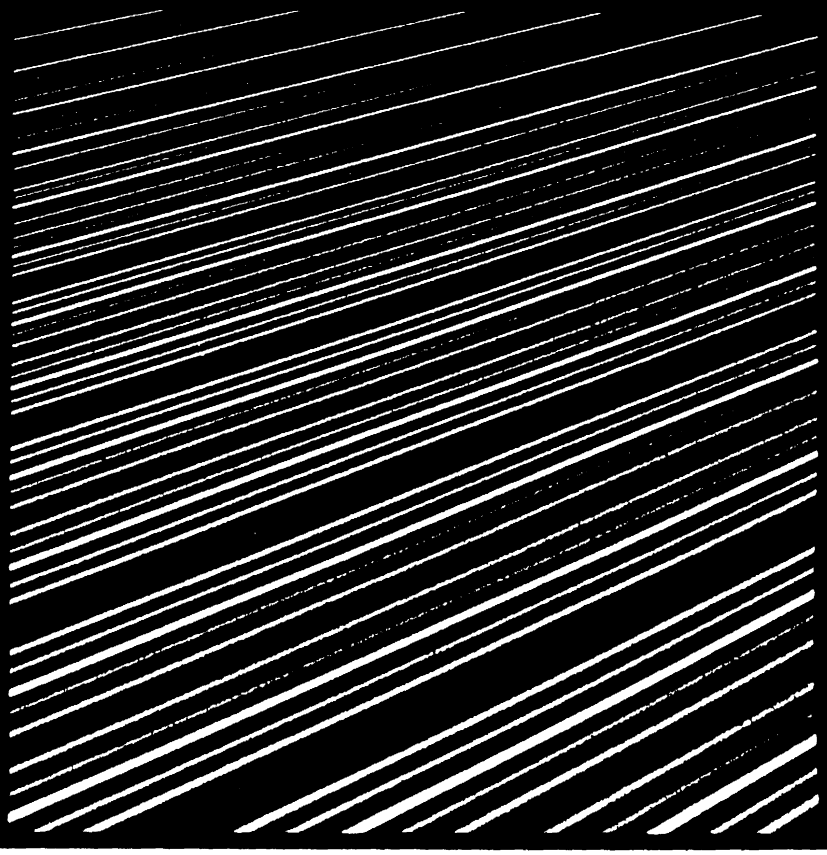

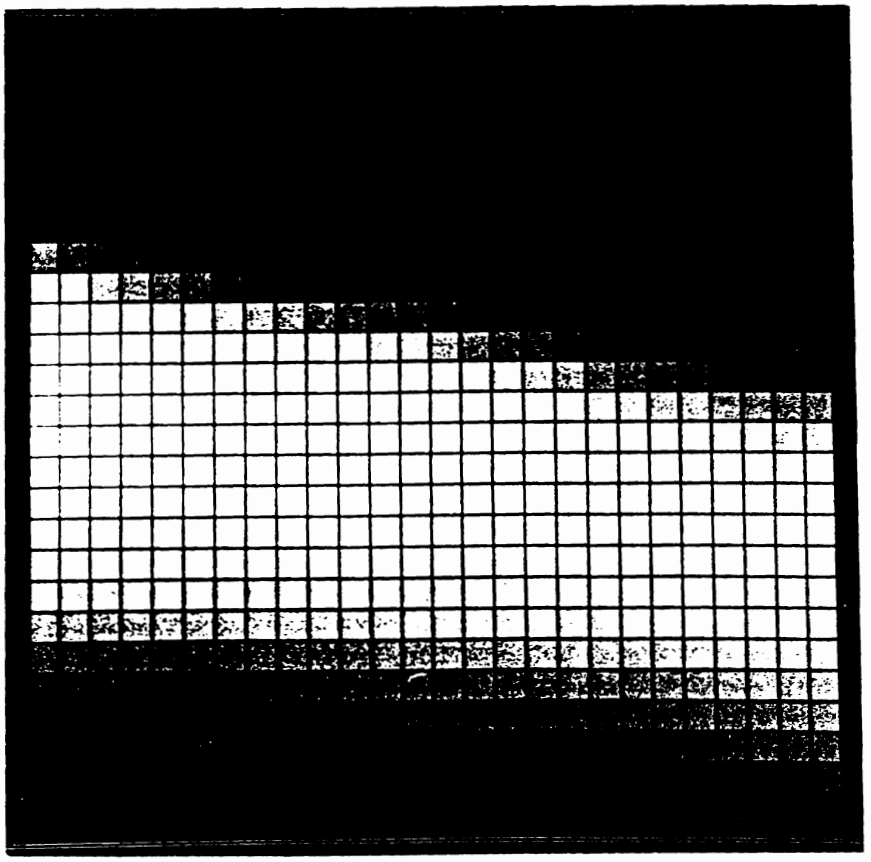

Figure 3b

Figure 3c

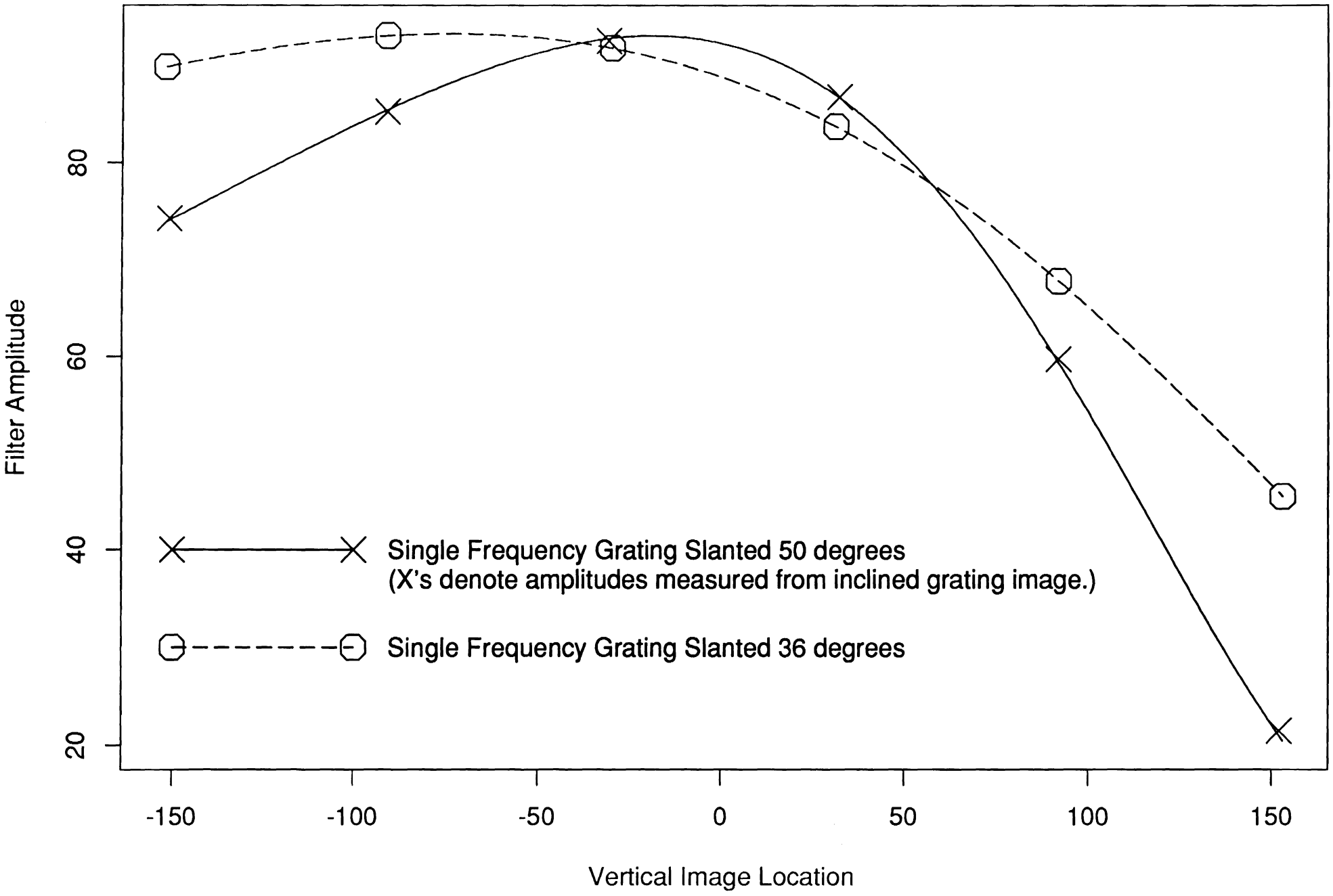
Filter Amplitude
20
40
60
80
-150
-100
-50
0
50
100
150
Vertical Image Location
Single Frequency Grating Slanted 50 degrees
(X's denote amplitudes measured from inclined grating image.)
Single Frequency Grating Slanted 36 degrees

Figure 3d

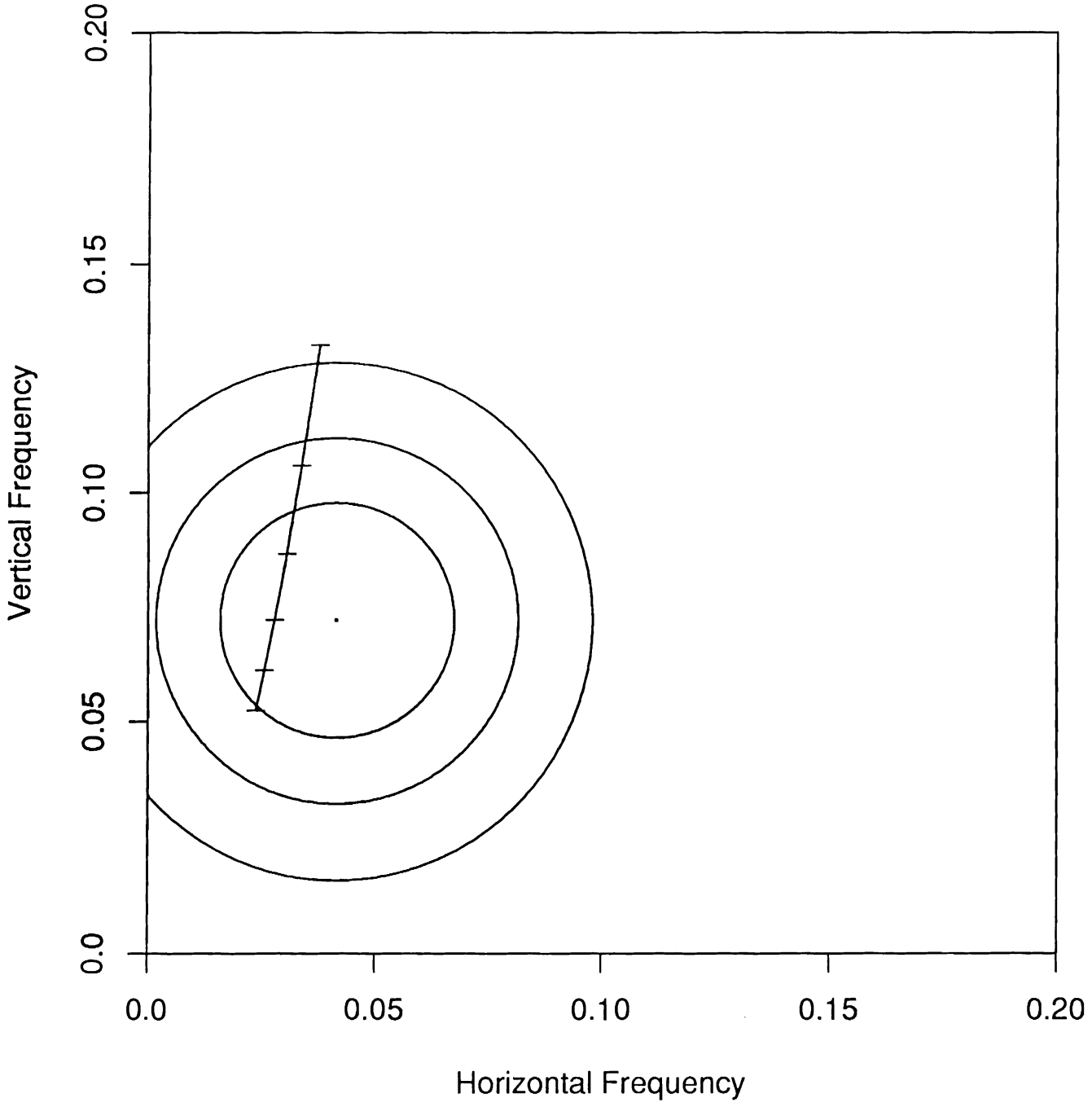
0.20
0.15
0.10
0.05
0.0
Vertical Frequency
0.0
0.05
0.10
0.15
0.20
Horizontal Frequency

Figure 4b

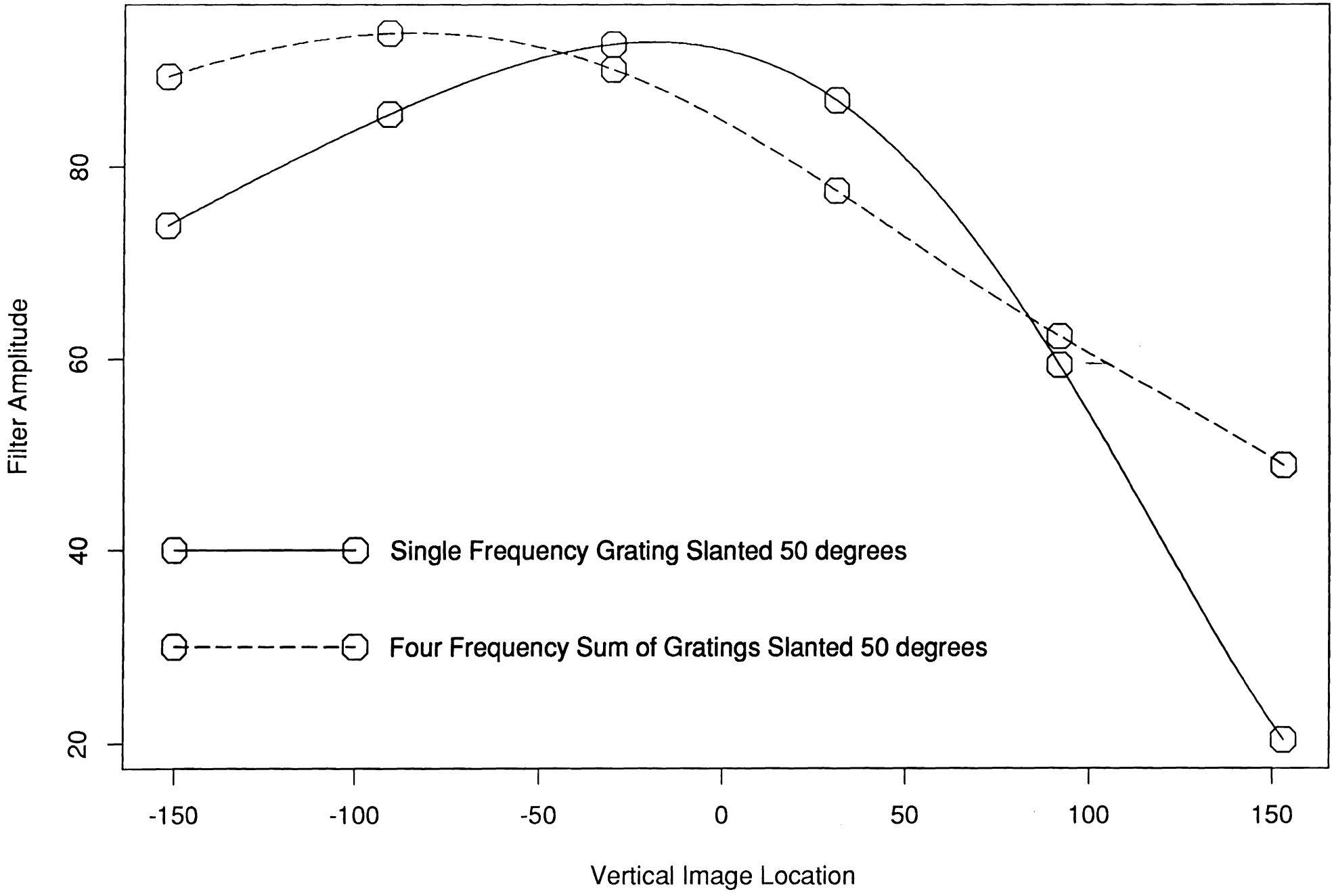
Filter Amplitude
20
40
60
80
-150
-100
-50
0
50
100
150
Vertical Image Location
Single Frequency Grating Slanted 50 degrees
Four Frequency Sum of Gratings Slanted 50 degrees

Figure 4c

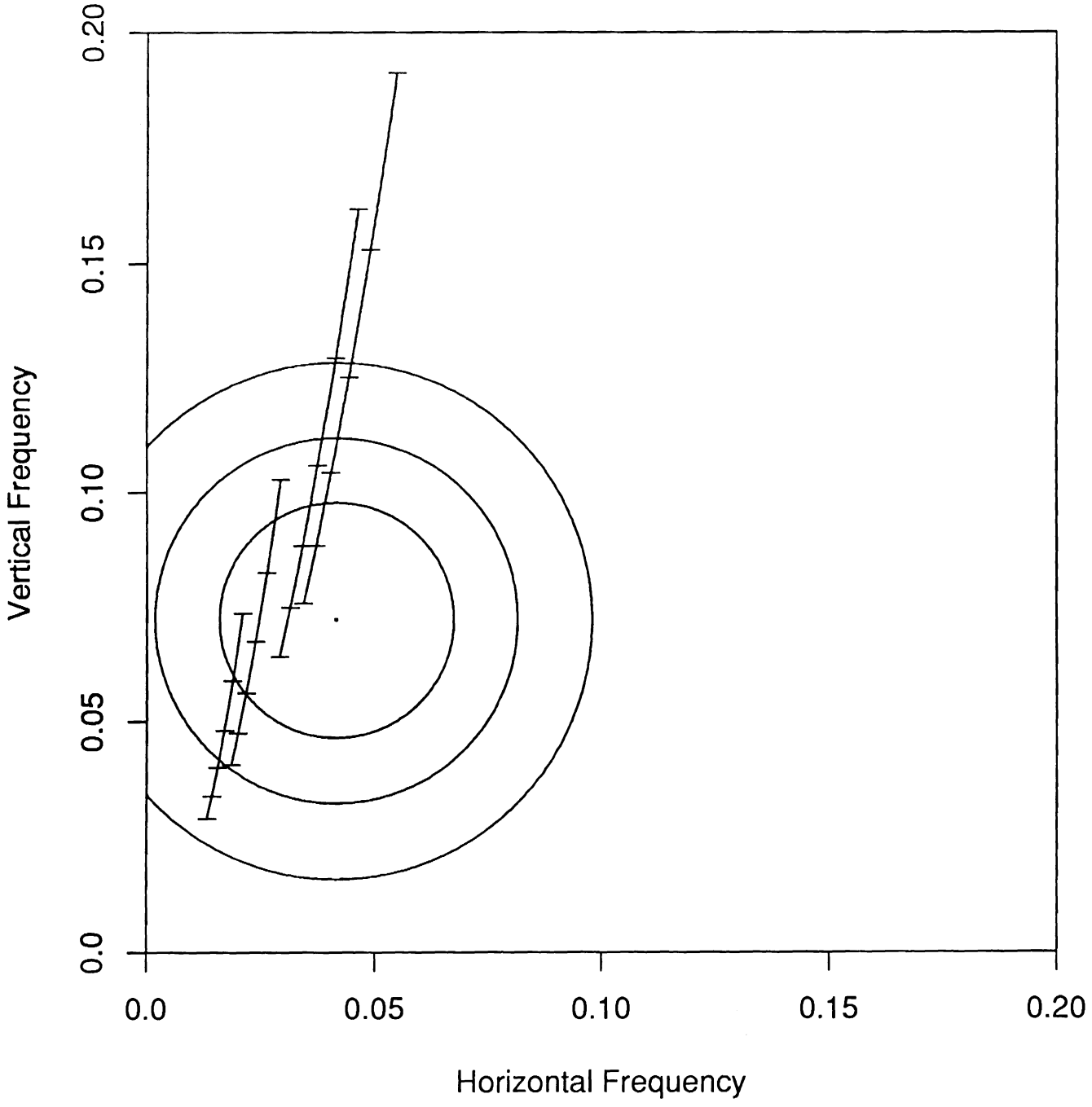
Vertical Frequency
0.0
0.05
0.10
0.15
0.20
0.0
0.05
0.10
0.15
0.20
Horizontal Frequency

Figure 5a

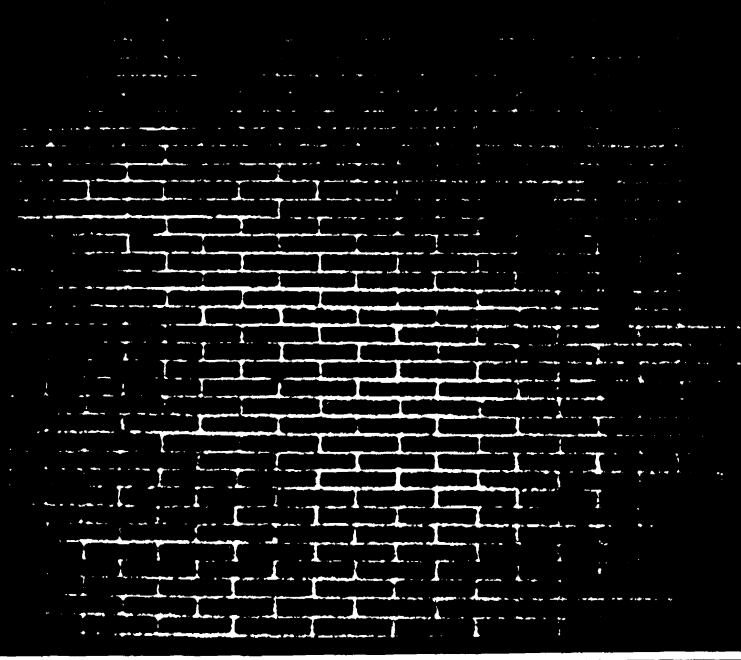

Figure 5c

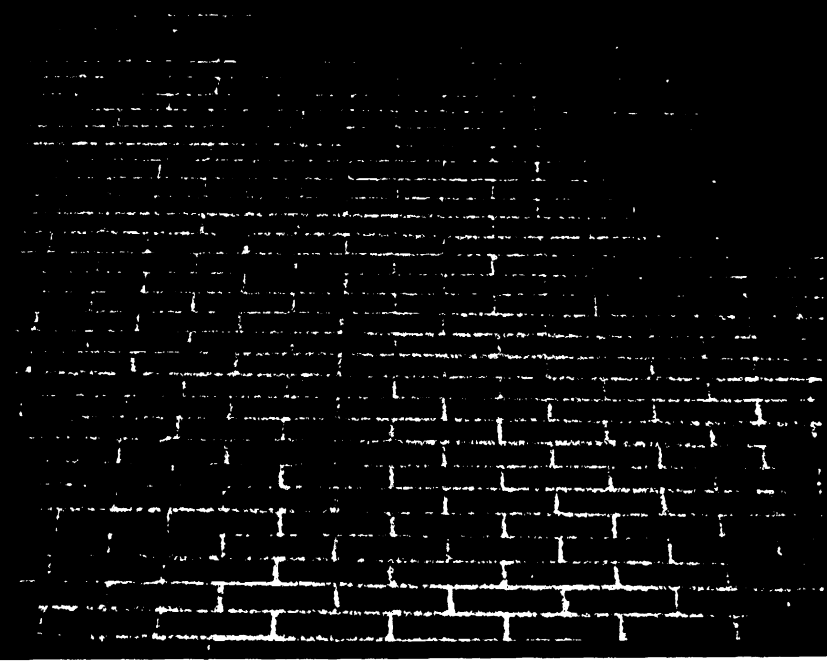

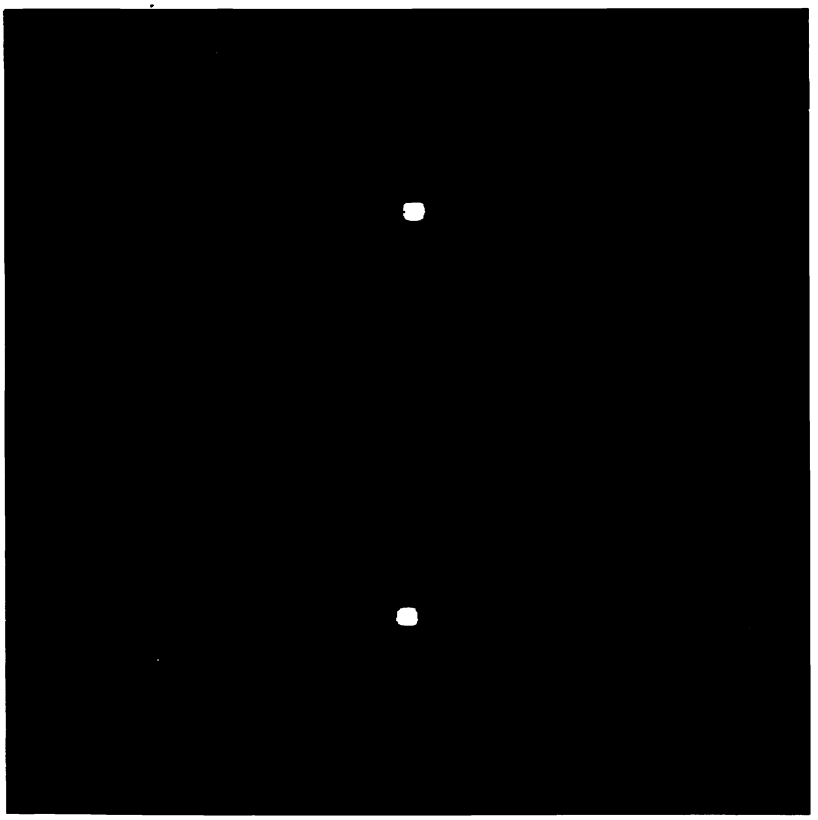

Figure 5b

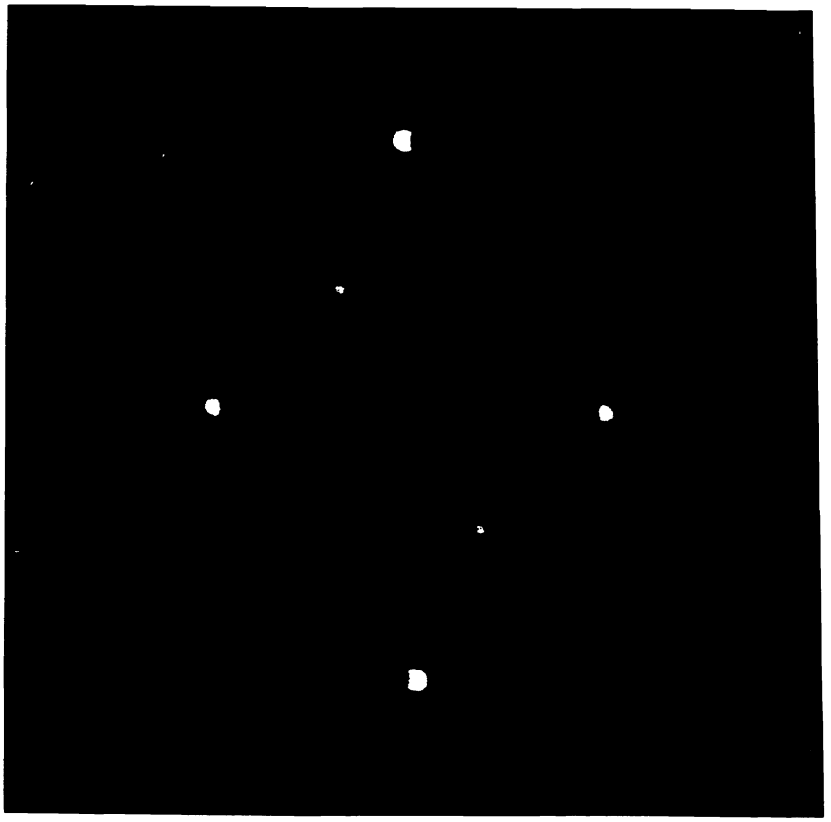

Figure 6b

Figure 6a

Figure 6c

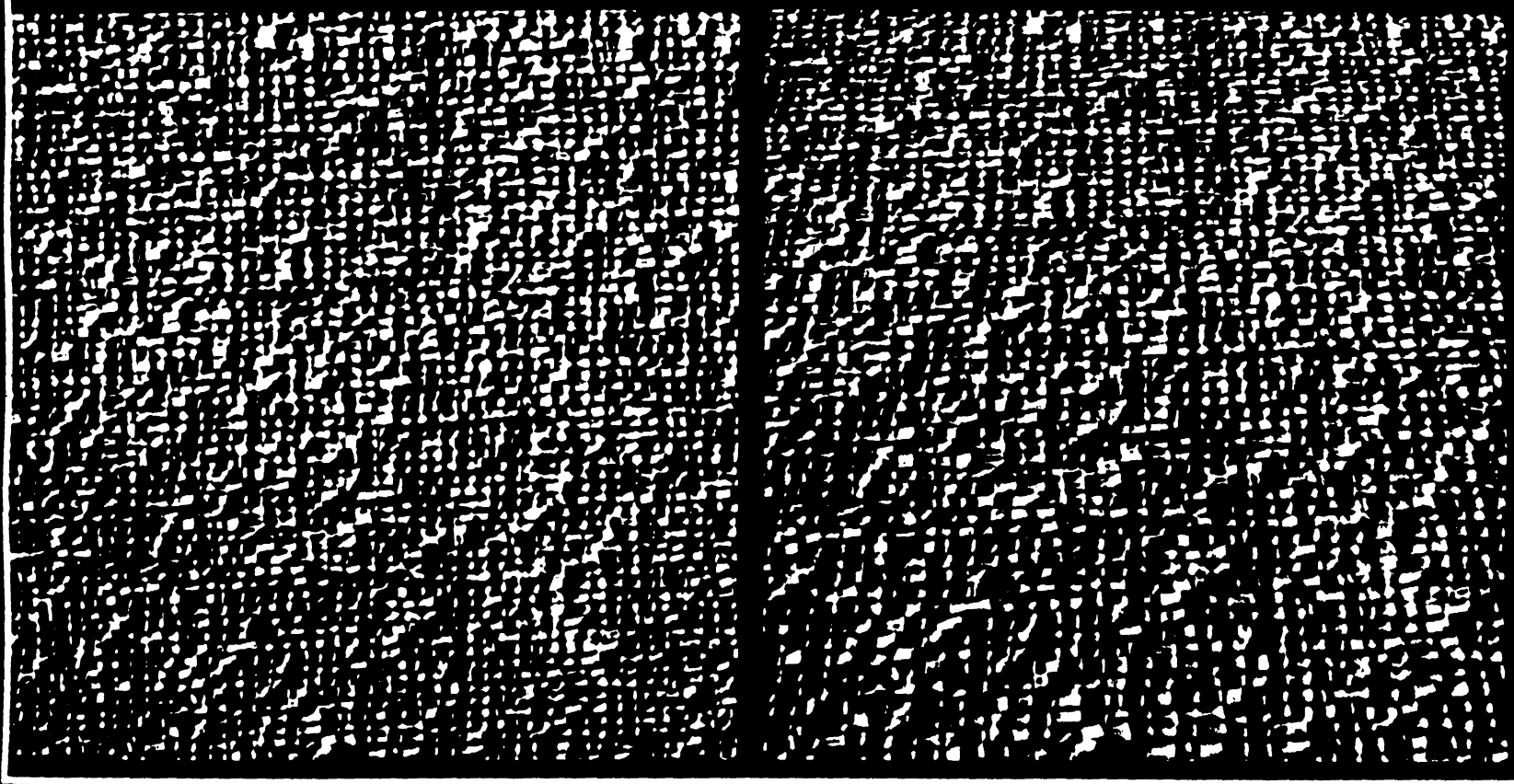

Figure 7a

Figure 7c

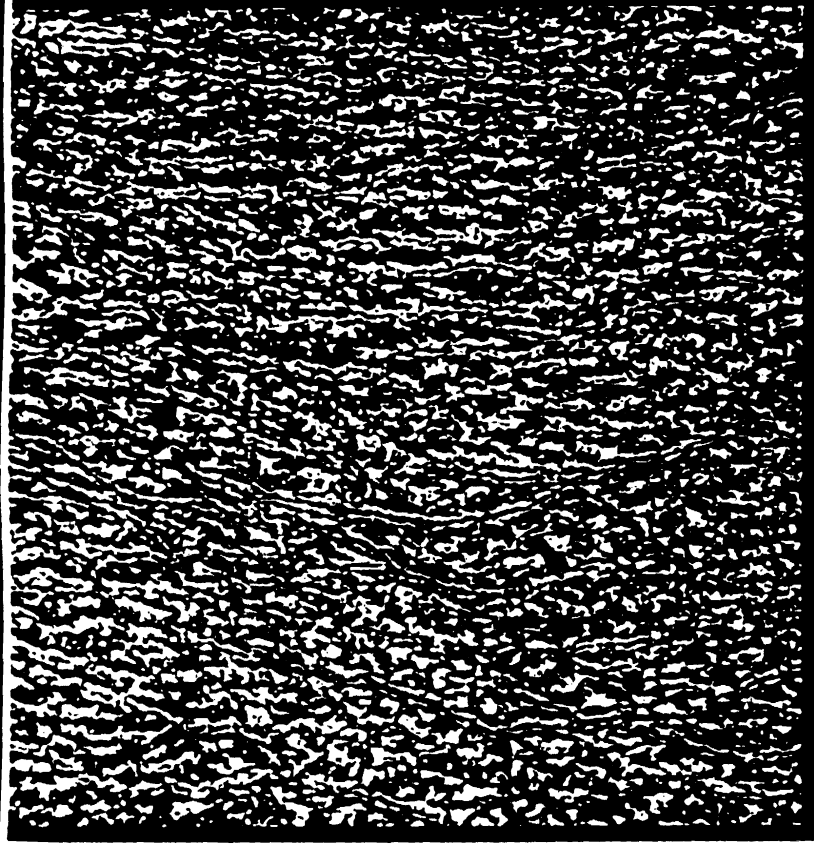

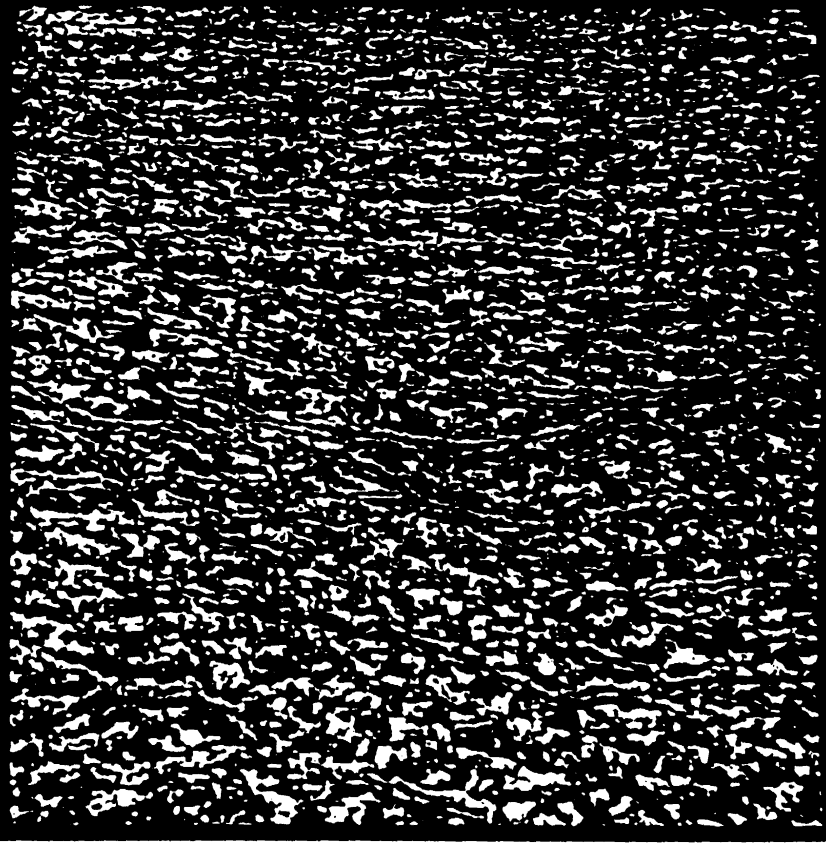

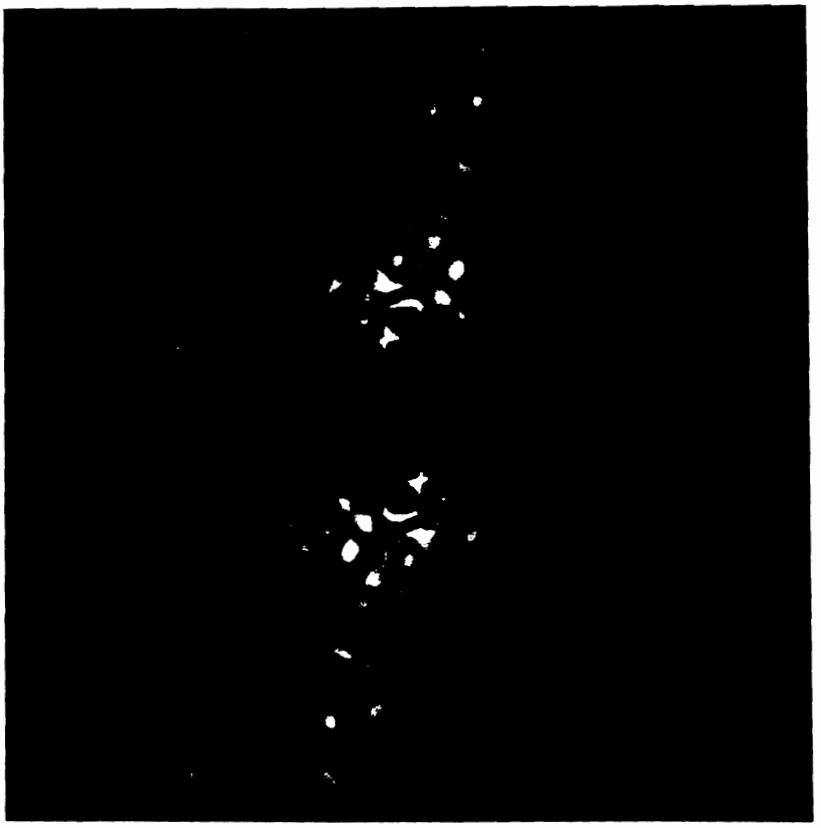

Figure 7b

Figure 8

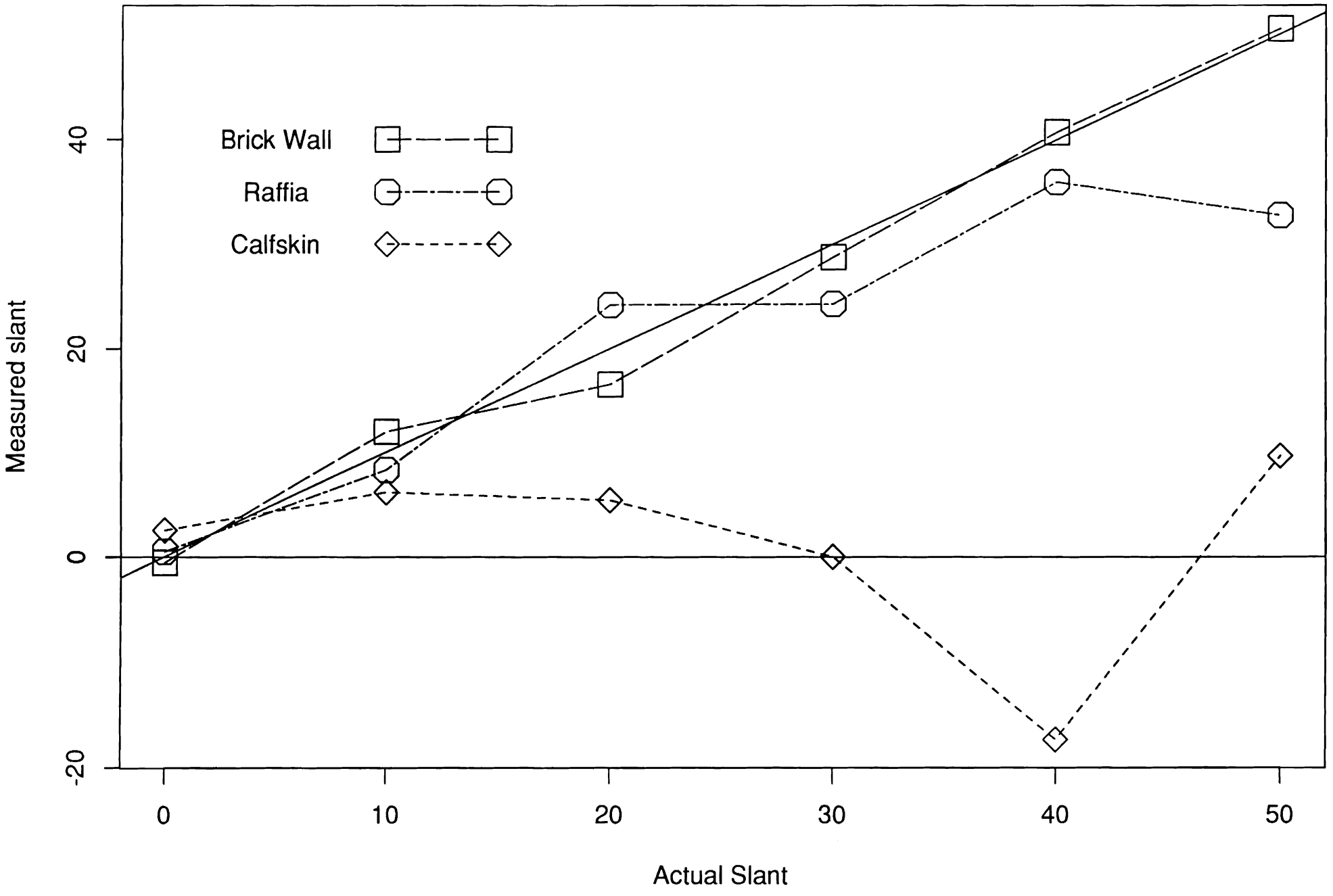
Brick Wall
Raffia
Calfskin
Measured slant
-20
0
20
40
0
10
20
30
40
50
Actual Slant